Geomechanics and Engineering, *Vol. 25, No. 3 (2021) 195-205*
DOI: https://doi.org/10.12989/gae.2021.25.3.195

Numerical study on the rate-dependent behavior of geogrid reinforced sand retaining walls

Fulin Li*[1,2], Tianran Ma[2a] and Yugui Yang[1b]

[1]*State Key Laboratory for Geomechanics and Deep Underground Engineering, China University of Mining and Technology, Xuzhou, Jiangsu 221116, P.R. China*
[2]*School of Mechanics and Civil Engineering, China University of Mining and Technology, Xuzhou, Jiangsu 221116, P.R. China*

(Received June 1, 2020, Revised April 3, 2021, Accepted April 15, 2021)

Abstract. Time effect on the deformation and strength characteristics of geogrid reinforced sand retaining wall has become an important issue in geotechnical and transportation engineering. Three physical model tests on geogrid reinforced sand retaining walls performed under various loading conditions were simulated to study their rate-dependent behaviors, using the presented nonlinear finite element method (FEM) analysis procedure. This FEM was based on the dynamic relaxation method and return mapping scheme, in which the combined effects of the rate-dependent behaviors of both the backfill soil and the geosynthetic reinforcement have been included. The rate-dependent behaviors of sands and geogrids should be attributed to the viscous property of materials, which can be described by the unified three-component elasto-viscoplastic constitutive model. By comparing the FEM simulations and the test results, it can be found that the present FEM was able to be successfully extended to the boundary value problems of geosynthetic reinforced soil retaining walls. The deformation and strength characteristics of the geogrid reinforced sand retaining walls can be well reproduced. Loading rate effect, the trends of jump in footing pressure upon the step-changes in the loading rate, occurred not only on sands and geogrids but also on geogrid reinforced sands retaining walls. The lateral earth pressure distributions against the back of retaining wall, the local tensile force in the geogrid arranged in the retaining wall and the local stresses beneath the footing under various loading conditions can also be predicted well in the FEM simulations.

Keywords: geogrid reinforced soil; retaining wall; numerical model; rate-dependent property; tensile force

1. Introduction

Polymer geosynthetics have been successfully used as reinforcement layers to support roadways, railways and bridge abutments (Han *et al.* 2018). Numerical simulation is one of the common and effective methods to predict the stress-strain behavior of geosynthetic reinforced soil structures, including the nonlinear elasto-plastic FEM and the discrete element method (DEM) (Karpurpu and Bathurst 1995, Chen *et al.* 2018, Elshesheny *et al.* 2020). In elasto-plastic FEM simulations, the backfill were usually described by either nonlinear elastic models, elastic-perfectly plastic models or associated/non-associated elasto-plastic models, while the geosynthetic reinforcements were described by linear or nonlinear elastic models. Rowe and Skinner (2001) performed a numerical research on geosynthetic reinforced retaining walls to examine the effect of the drained and undrained strength of the loam foundation material, its stiffness, the thickness of soft layer and its position. Villard *et al.* (2002) conducted elasto-plastic FEM simulations of a set of drained plane strain compression (PSC) test results, and the specimens were Toyoura sands either unreinforced or reinforced with one layer of various types of planar-reinforcement. Peng *et al.* (2000), using elasto-plastic FEM code, simulated the results from large-size PSC tests on Toyoura sands with 6 or 11 layers of geogrids. In these FEM analyses, the constitutive relations for sands were the elasto-plastic model which can take into account the strain localization and anisotropic stress-strain properties. The reinforcements were modeled by linear-elastic truss elements. By elasto-plastic FEM analysis, Kotake *et al.* (2002) simulated the results obtained from physical model tests on horizontal unreinforced and reinforced sand foundations. In this FEM simulation, the effects of the pressure-dependence of the friction angle, the strength anisotropy, the strain localization phenomenon, and the progressive failure were taken into account. Hosseinpour *et al.* (2014) used PLAXIS program to simulate the unit cell of the unreinforced and reinforced granular column, and conducted parametric analyses on geosynthetic reinforced granular columns, in which, the Hardening Soil model was adopted to describe soft clay and the Mohr-Coulomb model was used for both the granular column and the embankment fills.

However, as mentioned in Li *et al.* (2012), it has been proven that the geosynthetic reinforced soil structures are subjected to creep or stress relaxation due to the viscous properties of geosynthetic reinforcements. For geogrid-reinforced sand structures, more or less complicated stress-

*Corresponding author, Ph.D.
E-mail: lifulin@cumt.edu.cn
[a]Ph.D.
[b]Ph.D.

ISSN: 2005-307X (Print), 2092-6219 (Online)

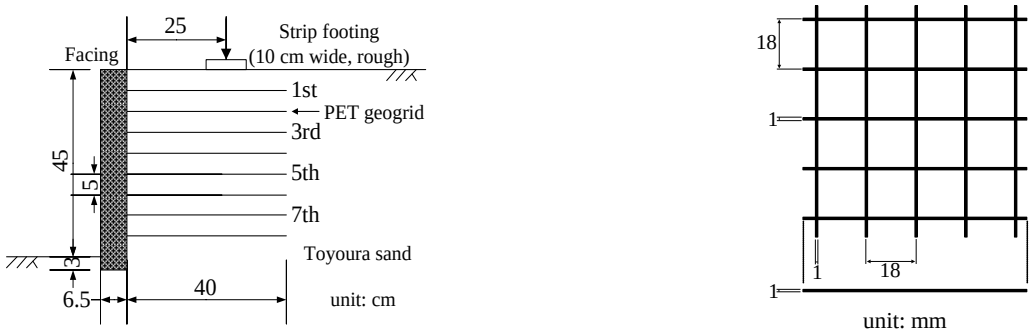

(a) Modeled retaining wall with geogrid layers (b) Details of PET geogrid

Fig. 1 Configurations of model tests on geogrid reinforced sand retaining walls (after Hirakawa (2003))

strain-time behaviors of sands (Kuwano and Jardine 2002, Van Bang *et al.* 2007, Lade *et al.* 2009, Pham Safa *et al.* 2019) or load-strain-time behaviors of geogrids (Bathurst *et al.* 2009, Rowe and Taechakumthorn 2011, Kongkitkul *et al.* 2014, Ezzein *et al.* 2015) were observed, including instantaneous nonlinearity and viscous effects. Because of the interactions between sands and geogrid reinforcements, the rate-dependent behaviors of geogrid reinforced sands may be very complicated (Tatsuoka *et al.* 2004). Liu and Won (2009) performed FEM analyses on the geogrid reinforced sand retaining walls, in which the creep and stress relaxation of geogrids were considered, while the backfill sands were described by elasto-plastic model. Shi *et al.* (2016) performed FEM analyses on geogrid reinforced sand in plane strain compression, in which an elasto-viscoplastic model was used for the geogrid, while the sand was modelled with an elasto-plastic model. Some studies have been reported for the simulation of the time-dependent behavior considering the viscous properties of both backfill and reinforcement (Liu *et al.* 2009, Rowe and Taechakumthorn 2011, Helwany and Wu 1995, Karim *et al.* 2011, Siddiquee *et al.* 2015), but the numerical research is not many on the behavior under loading at variable rates. Through incorporating the elasto-viscoplastic properties of both sands and polymer geogrids, Li *et al.* (2012) performed FEM simulations on geogrid reinforced sand under laboratory-scale PSC test results. It has been shown that the rate-dependent behavior, creep deformation and stress relaxation of geogrid reinforced sand can be realistically simulated, but these behaviors were not be validated by the FEM in the boundary value problems of geosynthetic reinforced soil.

In this study, a series of physical model tests under various loading conditions were simulated numerically to investigate the rate-dependent behaviors of geogrid reinforced sand retaining wall. The nonlinear FEM analysis technique incorporated the unified three-component elasto-viscoplastic constitutive model for both sands and geogrids. By comparing the results from the FEM analyses and the corresponding physical model tests, it is shown that the present FEM, considering the viscous properties of both the backfill and geosynthetic reinforcements, can be successfully extended to the boundary value problems of geosynthetic reinforced soil retaining walls. Not only the global load-deformation-time relationships but also the changing trends of the lateral earth pressure and the local tensile force of geogrid arranged in the retaining wall during loading, can be simulated well in the FEM analyses.

2. Physical model tests

A series of physical model tests on geogrid reinforced sand retaining wall were performed by Dr. Daiki Hirakawa under a plane strain condition reported in his Ph.D. Thesis (Hirakawa 2003). The tests were carried out in the Geotechnical Laboratory, Department of Civil Engineering at the University of Tokyo, under supervision of Prof. Fumio Tatsuoka. The results of three physical model tests, numbered as RW-Test1, RW-Test2 and RW-Test3, were analyzed in this numerical study. The experimental apparatus consisted of a vertical loading system, a sand box, a scaled-down geogrid reinforced sand retaining wall model and a 10 cm-wide strip footing. The sand box was 180 cm long, 40 cm wide and 80 cm high inside, and the inner faces of the sidewalls of the sand box were lubricated with a 0.3 mm-thick latex membrane sheet smeared with 15 μm-thick Dow high vacuum silicone grease. The model was built in the sand box by tamping air-dried Toyoura sand (specific gravity G_s = 2.65, maximum void ratio e_{max} = 0.933, and minimum void ratio e_{min} = 0.624) in eight layers to obtain a relative density D_r = 90 % (initial void ratio e_0 = 0.65 and dry unit weight γ_d = 16.0 kN/m^3). The model retaining wall was 48 cm high with an embedment depth of 3 cm, which was embedded into a 25 cm-thick sand layer in the sand box, see Fig. 1(a). It was assumed that the model size was 1/6 of a typical prototype reinforced retaining wall. The backfill sand was reinforced with 8 layers of polyester (PET) geogrids with a centre-to-centre grid spacing equals to 18 mm, see Fig. 1(b). The covering ratio (*CR*) of PET geogrid was defined as the ratio of the area of the reinforcement covering a given plane to the area of the plane, and the *CR* was 11.1 % in the present study. The back face of the full-height rigid facing was made rough by gluing sandpaper.

To obtain the distributions of earth pressures of the retaining wall, several load cells were arranged at the back face of the facing. Local tensile strains in the reinforcement were measured with electric-resistance strain gauges at the 5th reinforcement layer. The models were vertically loaded

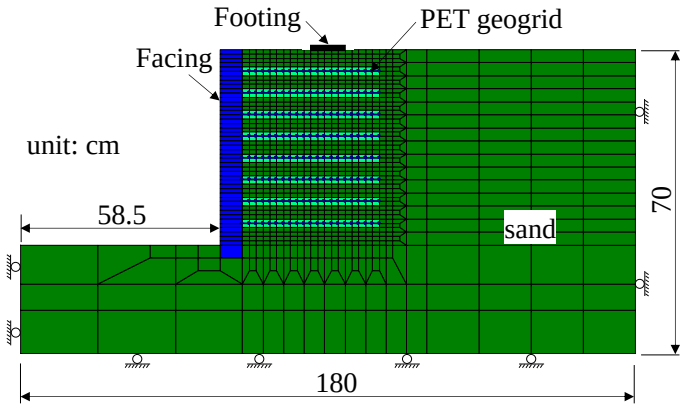

Fig. 2 FEM mesh

through a 10 cm-wide rigid strip footing with rough bottom face. The distance was 25 cm from the back face of the facing to the central axis of footing. To observe the progressive failure of the backfill, five two-component load cells, similar to those arranged at the back face of the facing, were arranged at the footing base. A unique gear-type axial loading device was used to apply vertical load, in which the vertical displacement rate was controlled within a resolution of less than one μm and the loading direction was reversed without backlash. In the tests, the vertical settlement rate of the footing was changed stepwise many times in a range from 4.72×10^{-3} mm/min to 4.72×10^{-1} mm/min by a factor of upto 100. The stress relaxation stages, small cyclic loading stages and creep loading stages could also be carried out during loading in different tests. During these physical model tests, no pronounced slippage between sands and geogrids was observed, and no geogrids were pulled out.

3. Numerical modeling

3.1 FEM model

The FEM code based on the dynamic relaxation technique (Tanaka and Kawamoto, 1988) and return mapping scheme (Ortiz and Simo, 1986) was used in the present study. The dynamic relaxation technique and the return mapping scheme were used to solve the nonlinear equation groups and to update the stress, respectively. In the presence of the strong material nonlinearity due to the granular material with a high friction angle such as sands, the dynamic relaxation technique has a prodigious reputation in solving highly nonlinear equations (Siddiquee *et al.* 1995). By using the return mapping, the updated elasto-plastic solution was obtained; and then the corresponding elasto-viscoplastic solution was calculated. To ameliorate the bounds of solution in the pseudo-equilibrium, 4-node quadrilateral elements with reduced integration were adopted in the FEM. Hence, a very small elastic stiffness of the actual material elastic stiffness at the start of loading was added to the nonlinear system as hourglass resisting nodal forces whenever any soil element starts to form an hourglass mode. The FEM code has been validated by simulating the rate-dependent behavior on unreinforced and geosynthetic reinforced sands (Siddiquee *et al.* 2006, Peng *et al.* 2010, Li *et al.* 2012).

According to the physical model tests, the FEM mesh of geogrid reinforced sand retaining wall was shown in Fig. 2. Four-node quadrilateral plane elements were selected to simulate the backfill and the facing. The PET geogrid layers were simulated by nonlinear truss elements. The regions, where geogrid reinforcements were placed, were refined into relatively small elements, while the unreinforced regions were discretized into relatively coarse elements. The total numbers of the elements and the nodal points were 1435 and 1335, respectively. The bottom and lateral boundaries of the FEM model were set as horizontal and vertical rollers, respectively. This should be much more representative than fixed boundaries to simulate the one in the physical model test.

A unit weight of dry sand γ_d of 16.0 kN/m^3 and an initial void ratio e_0 of 0.65, which are the same as the values used in the experiment, were used in the FEM simulation. The initial stress state of the retaining wall model was approximately assumed to be under the K_0-stress condition with K_0=0.34, in which K_0 is the coefficient of earth pressure at rest. Vertical settlement vectors were assigned to the nodes at the footing base tracing the measured time history of footing settlement in the physical model test. No lateral movement of those nodal points was allowed so as to simulate perfectly rough base conditions. Meanwhile, the creep loading was simulated under stress-controlled conditions using the measured time histories of stresses (i.e., $\dot{\sigma}$= 0).

3.2 A brief explanation of constitutive model

In rheology of geomaterials, rheological models include not only viscoelastic but also plastic behaviors. One of the most important methods to compose constitutive relations is to combine different elementary material components, such as Hookean spring, Newtonian dashpot and Saint-Vernant's slider, in series and/or parallel. Three-component model can be considered as a typical constitutive model of this type of rheological models. In the framework of a three-component model, component 1 connects in series with a parallel unit

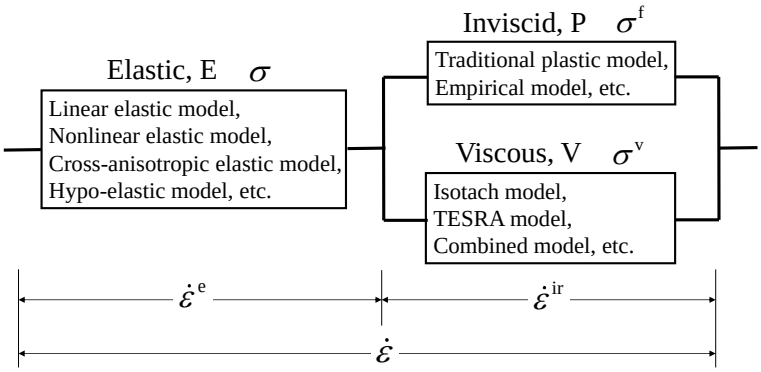

Fig. 3 Framework of three-component elasto-viscoplastic model

composed of component 2 and component 3 (Fig. 3). The Bingham model, for example, is a three-component model, in which components 1, 2 and 3 are a linear spring, a plastic slider and a linear dashpot, respectively.

A general nonlinear three-component elasto-viscoplastic model was developed by Di Benedetto *et al.* (2002) and Tatsuoka *et al.* (2002) as shown in Fig. 3. Three components were denoted as an elastic component E, a nonlinear inviscid component P, and a nonlinear viscous component V, respectively. For the three-component model described above, the total stress, σ, consists of nonlinear inviscid and viscous components, σ^{f} and σ^{v}, while the total strain rate, $\dot{\varepsilon}$, consists of elastic and irreversible components, $\dot{\varepsilon}^{e}$ and $\dot{\varepsilon}^{ir}$, which can be expressed as:

$$\dot{\varepsilon} = \dot{\varepsilon}^{e} + \dot{\varepsilon}^{ir} \tag{1}$$

$$\sigma = \sigma^{f} + \sigma^{v} \tag{2}$$

The elastic component E can be described by an elastic model that is relevant to a given material type, such as linear elastic model, nonlinear elastic model, cross-anisotropic elastic model, hypo-elastic model, and so on. Traditional plastic models and reasonable empirical models contribute to the nonlinear inviscid component P. The nonlinear viscous component V is used to represent the rate-dependent stress-strain behavior of geomaterials. It has been found that there are at least three types of viscous properties, including isotach viscosity, TESRA (Temporary Effects of Strain Rate and Acceleration) viscosity, and combined viscosity (Hirakawa *et al.* 2003). The corresponding rate-dependent viscous models for component V can be called the isotach model, the TESRA model, and the combined model, which can be expressed as:

$$\sigma^{v} = \begin{cases} \sigma^{v}_{iso} = \sigma^{f}(\varepsilon^{ir}) \cdot g_{v}(\dot{\varepsilon}^{ir}) & \text{(isotach model)} \\ \sigma^{v}_{TESRA} = \int_{\tau=\varepsilon^{ir}_{i}}^{\varepsilon^{ir}} [d\sigma^{v}_{iso}]_{(\tau)} \cdot r_{d}^{(\varepsilon^{ir}-\tau)} & \text{(TESRA model)} \\ \sigma^{v}_{com} = \lambda^{v} \cdot \sigma^{v}_{iso} + (1-\lambda^{v}) \cdot \sigma^{v}_{TESRA} & \text{(combined model)} \end{cases} \tag{3}$$

where, $g_{v}(\dot{\varepsilon}^{ir})$ is the viscosity function and given as follows for any strain history:

$$g_{v}(\dot{\varepsilon}^{ir}) = \alpha\{1 - \exp[1 - (|\dot{\varepsilon}^{ir}| / \dot{\varepsilon}^{ir}_{r} + 1)^{m}]\} \tag{4}$$

Table 1 Rate-dependent model parameters for Toyoura sand and PET geogrid

Material type	α	m	$\dot{\varepsilon}^{ir}$ (%/s)	r_{d}	λ^{v}
Toyoura sand	0.23	0.045	10^{-6}	0.2	0
PET geogrid	0.7	0.12	10^{-4}	$0.575 + 0.425\cos[\pi(\varepsilon^{ir} / 0.4)^{0.6}]$	0.8

The rate-dependent viscous model presents a rule that the viscous stress is obtained by scaling the inviscid stress according to the irreversible strain rate. The scaling factor in isotach model is the viscosity function, where α, m and $\dot{\varepsilon}^{ir}_{r}$ are the positive material constants. The effects of irreversible strain rate and its rate (i.e. irreversible strain acceleration) on the stress-strain relationship are permanent according to the isotach viscosity, such as clay and soft rock. For the TESRA viscosity, the effects of irreversible strain rate and its rate on the stress-strain relationship become temporary, which exhibits the stress overshooting or undershooting phenomena such as sands. r_{d} is the decay parameter. The combined model, considering the features of both isotach and TESRA models, can be used to describe the rate-dependent viscous property of PET geogrid. λ^{v} is a material constant to determine the type of rate-dependent viscous properties. When λ^{v} is equal to 1 and 0, the combined viscosity becomes the isotach and TESRA viscosities, respectively. The parameters of rate-dependent viscous model can be determined from the variable loading rate tests.

The FEM code embedded with the nonlinear three-component elasto-viscoplastic model, which is able to describe stress-strain-time properties of geomaterials, especially for the rate-dependent behaviors, was used in the present study. For both sands and geosynthetic reinforcements, the elastic component E is the cross-anisotropic hypo-elastic model (Hoque and Tatsuoka 1998).

For sands, the nonlinear inviscid component P is described by an isotropic, work-hardening and softening, and non-associated plastic model, which takes the modified irreversible strain energy as the work-hardening parameter. It has been demonstrated that this plastic model can describe the deformation and strength characteristics of sands influenced by stress path, pressure level, void ratio, inherent anisotropy, and work-softening associated with

Table 2 Various loading histories in the physical model tests

Test name	Details of loading histories
RW-Test1	b-c, d-e, f-g, h-i, j-k, l-m, n-o, p-q, r-s, t-u, v-w, x-y, z-A, B-C: $\dot{s}^*$ a-b, e-f, i-j, m-n, q-r, u-v, y-z: 10 $\dot{s}$ c-d, g-h, k-l, o-p, s-t, w-x, A-B: 100 $\dot{s}$
RW-Test2	b-c, f-g: $\dot{s}$ a-b, d-e, g-h, i-j, k-l, p-q, r-s: 10 $\dot{s}$ c-d, e-f: 100 $\dot{s}$ h-i: Creep (for 2 h) j-k: Relaxation (for 2 h) l-m, o-p: Creep (for 6 h) m-n: Cyclic, q=12.67 kPa, 300 times, 10 $\dot{s}$ n-o: Cyclic, q=38.01 kPa, 300 times, 10 $\dot{s}$ q-r: Cyclic, q=25.34 kPa, 100 times, 10 $\dot{s}$ s-t: Relaxation (for 10 h)
RW-Test3	a-b, d-e, f-g, h-i, i-j, k-l, m-n, o-p, q-r, s-t, u-v, w-x, z-A, B-C, C-D, E-F, G-H, I-J, K-L, N-O, P-Q, R-S, T-U, W-X: 10 $\dot{s}$ b-c: $\dot{s}$ c-d, e-f, p-q, A-B, J-K: 100$\dot{s}$ g-h, r-s, t-u: Creep (for 1 h) x-y, L-M, U-V: Creep (for 6 h) j-k, l-m, n-o, D-E, F-G, H-I, O-P, Q-R, S-T, X-Y: Creep (for 0.5 h) v-w: Relaxation (for 0.5 h) y-z, M-N, V-W: Cyclic, q=25.34 kPa, 500 times, 100 $\dot{s}$

* $\dot{s}$: $\dot{s} = 4.72\times10^{-3}$ mm/min

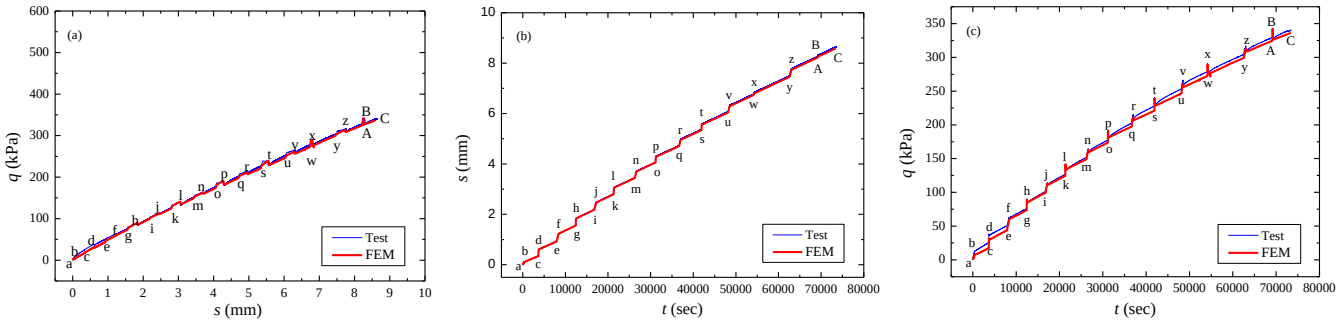

(a) q-s relationship (b) Time history of s (c) Time history of q

Fig. 4 Measured and FEM simulated results from the physical model test (RW-Test1)

strain localization into a shear band (Peng *et al.* 2009). The TESRA model for nonlinear viscous component V is adequate for simulating the viscous properties of Toyoura sand in the present FEM analysis.

For geosynthetic reinforcements, the nonlinear inviscid component P can be simply expressed as a polynomial function, based on the results from tensile tests at a constant stain rate. The combined model for nonlinear viscous component V is adequate for simulate the viscous properties of PET geogrid. The details of the nonlinear three-component elasto-viscoplastic model and the corresponding material parameter determination can be found in Peng *et al.* (2009) and Hirakawa *et al.* (2003) for Toyoura sand and PET geogrid, respectively. The parameter determination method of rate-dependent model can also be referred to Di Benedetto *et al.* (2002) and Tatsuoka *et al.* 2002. Rate-dependent model parameters for Toyoura sand and PET geogrid used in the FEM simulation are summarized in Table 1.

For the interface between sands and geogrids, considering neither pronounced slippage between sands and geogrids nor pullout failure of geogrids observed in the physical model tests, the present FEM analyses do not use the particular interface elements. It has been found that, compared to those in contact with a plate reinforcement layer, the average shear strength of sands in contact with a grid reinforcement layer is weaker under the otherwise same conditions. With the *CR* of geogrid increases, the average shear strength along the interface increases. In the present FEM analyses, it is a weaker factor of 0.72 was set up on the strength of sand elements in the respective layer in contact with geogrid, which is lower than the original value of other backfill. This factor was determined based on the *CR*-equivalent interface angle proposed in the study of Peng *et al.* (2000). When no pronounced slippage between sand and reinforcement and pullout failure of reinforcement was observed in the tests, this method is only a small part of the causes for the discrepancy between the FEM analysis and the test. This modeling method was also used in the elasto-plastic or elasto-viscoplastic FEM analyses on reinforced sand performed by Peng *et al.* (2000), Kotake *et al.* (2002), and Li *et al.* (2012).

4. Results and discussions

4.1 Global load-deformation-time relationships

The FEM simulated q-s-t relationships with the

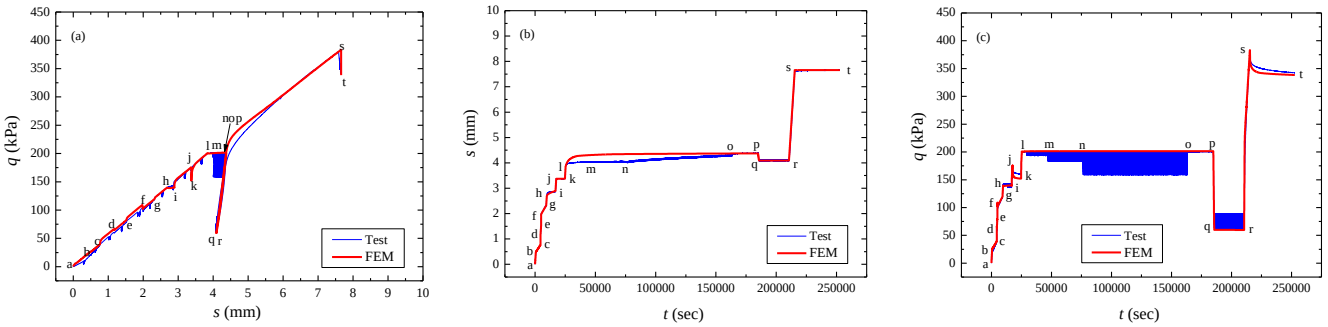

(a) *q*-*s* relationship (b) Time history of *s* (c) Time history of *q*

Fig. 5 Measured and FEM simulated results from the physical model test (RW-Test2)

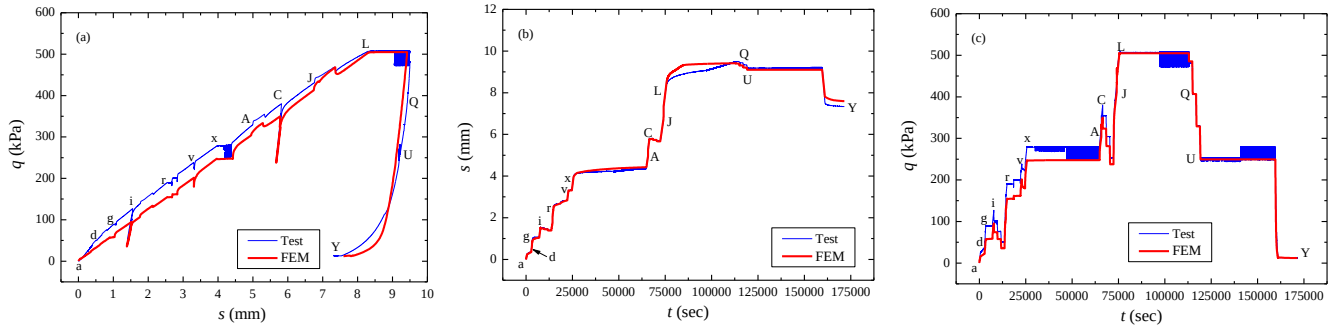

(a) *q*-*s* relationship (b) Time history of *s* (c) Time history of *q*

Fig. 6 Measured and FEM simulated results from the physical model test (RW-Test3)

experimental results are shown in Figs. 4-6 according to the physical model tests RW-Test1, RW-Test2 and RW-Test3, where *q* is the average vertical pressure of footing, *s* is the footing settlement, and *t* is the time. In Figs. 4-6, figures (a), (b) and (c) show the *q*-*s* relationships, the time history of *s,* and the time history of *q*, respectively. The details of loading history for RW-Test1, RW-Test2 and RW-Test3 were listed in Table 2.

By comparing the measured data with the FEM simulated results, it can be seen that not only the global *q*-*s*-*t* behaviors but also rate-dependent behaviors are well simulated. In particular, the simulated results exhibit an obvious trend of behavior with the high stiffness upon the stepwise in the loading rate, after the creep loading stages and stress relaxation stages, which are similar to those observed in the physical model test. This behavior is very similar to those of Toyoura sand (Tatsuoka *et al.* 2002) and PET geogrid (Hirakawa *et al.* 2003). It is shown that the rate-dependent behaviors and the deformation characteristics during sustained loading of geogrid reinforced sand retaining wall can be simulated rationally by the presented FEM analysis technique through integrating the elasto-viscoplastic properties of both backfill and geogrid reinforcement. Due to the similar features of residual deformation, the FEM simulations of cyclic loading are simulated by assuming a creep loading for the same period. That is, the cyclic loading stages (RW-Test2: m→o, q→r; RW-Test3: y→z, M→N, V→W) were replaced by creep loading stages with the same time interval for simplification. The general results of simulations are generally acceptable.

4.2 Lateral earth pressure

Fig. 7 compares the distribution of FEM-simulated lateral earth pressure against wall back, σ_h, along the depth, *h*, from the wall crest during the physical model test RW-Test1. The states e, h, k, n, q, t, w, and z in Fig. 4 are selected for analysis. The experimental results are presented as well.

By comparing the FEM simulation and experimental results, it can be seen that the FEM simulated lateral earth pressures at wall back are in good agreement with the measured values in the physical model test in terms of both the distribution patterns and the magnitudes, especially in a period immediately after loading start. The distribution patterns of lateral earth pressures from both FEM simulation and physical model test exhibit a triangle, the lateral earth pressure increases as the depth from the wall crest increases. The FEM simulation can successfully capture the features of lateral earth pressure at wall back, such as the distribution pattern and the moving trend of the maximum value of lateral earth pressures.

4.3 Tensile force in geogrid reinforcement

Fig. 8 compares the distribution of FEM simulated and measured local tensile force, T_{local}, of the 5th layer geogrid from the wall crest during the physical model test RW-Test3. The states d, g, i, r, v, x, C, and L in Fig. 6 are selected for analysis. The experimental results are also presented for reference.

It can be seen in Fig. 8 that the distribution patterns of

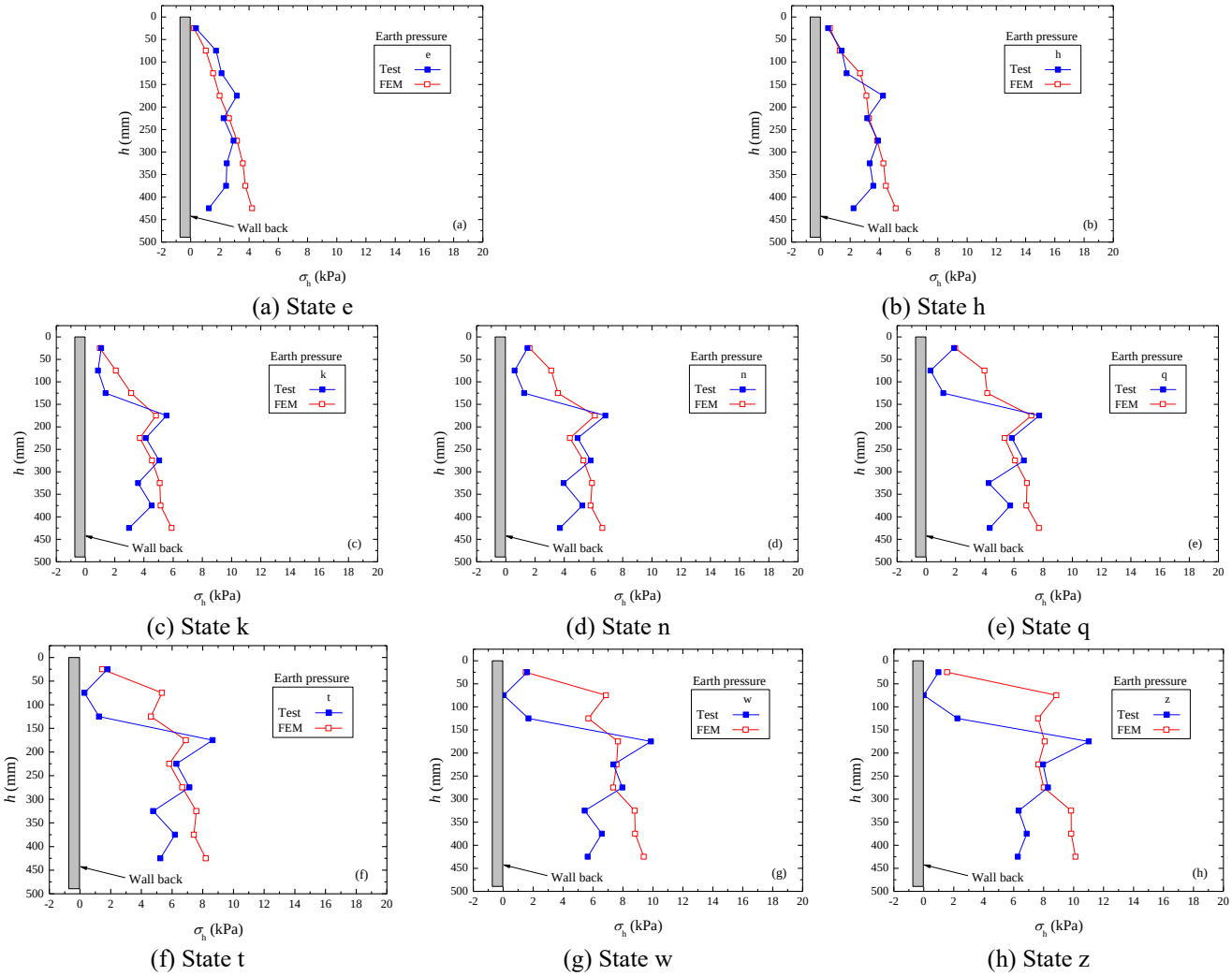

(a) State e (b) State h

(c) State k (d) State n (e) State q

(f) State t (g) State w (h) State z

Fig. 7 FEM simulated and measured wall back earth pressures during RW-Test1

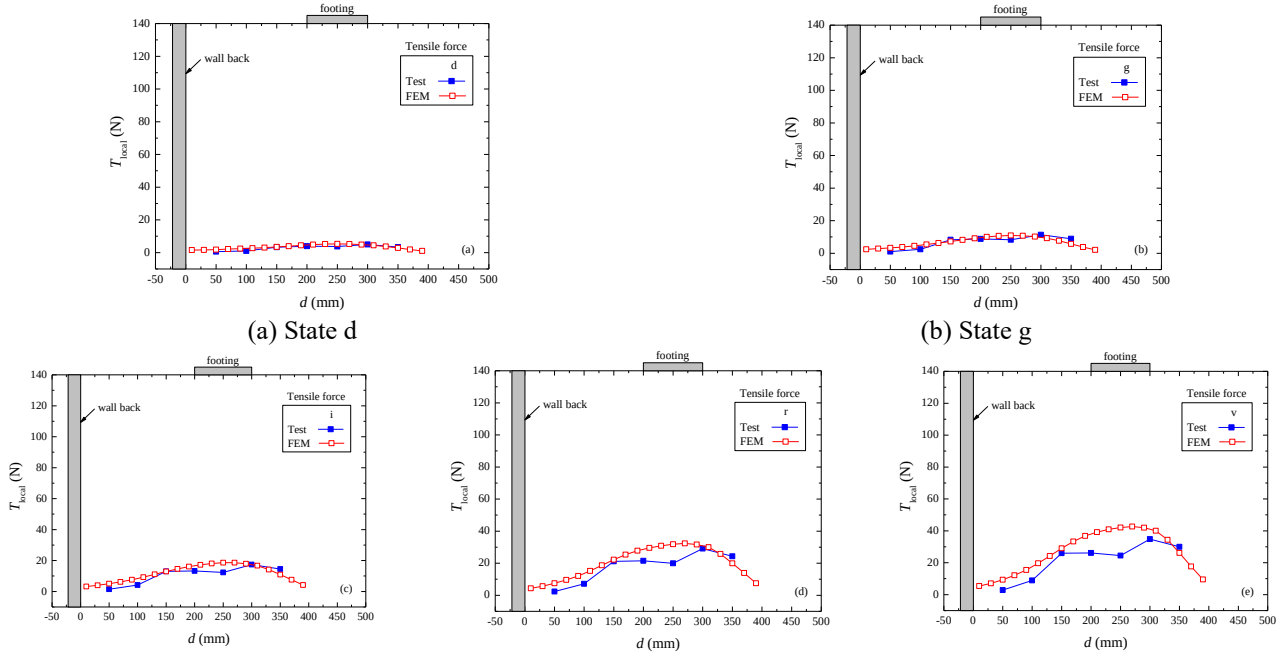

(a) State d (b) State g

(c) State i (d) State r (e) State v

Fig. 8 FEM simulated and measured tensile forces in the 5th layer geogrid during RW-Test3

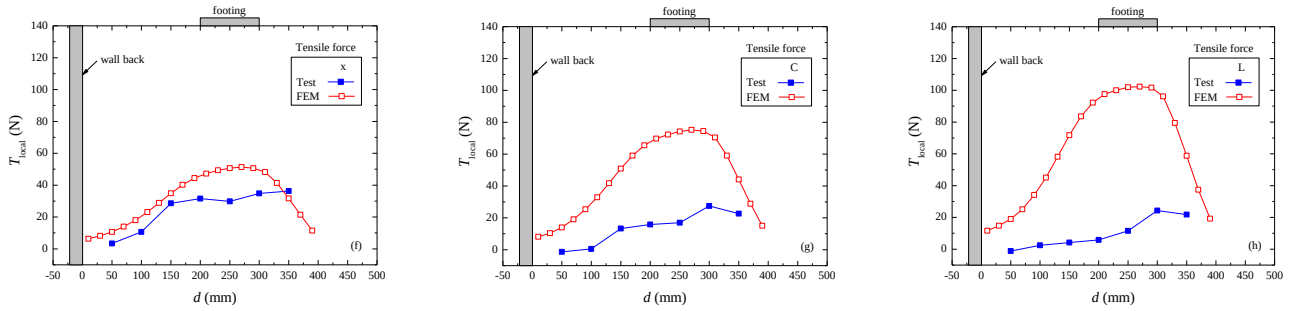

(f) State x (g) State C (h) State L

Fig. 8 Continued

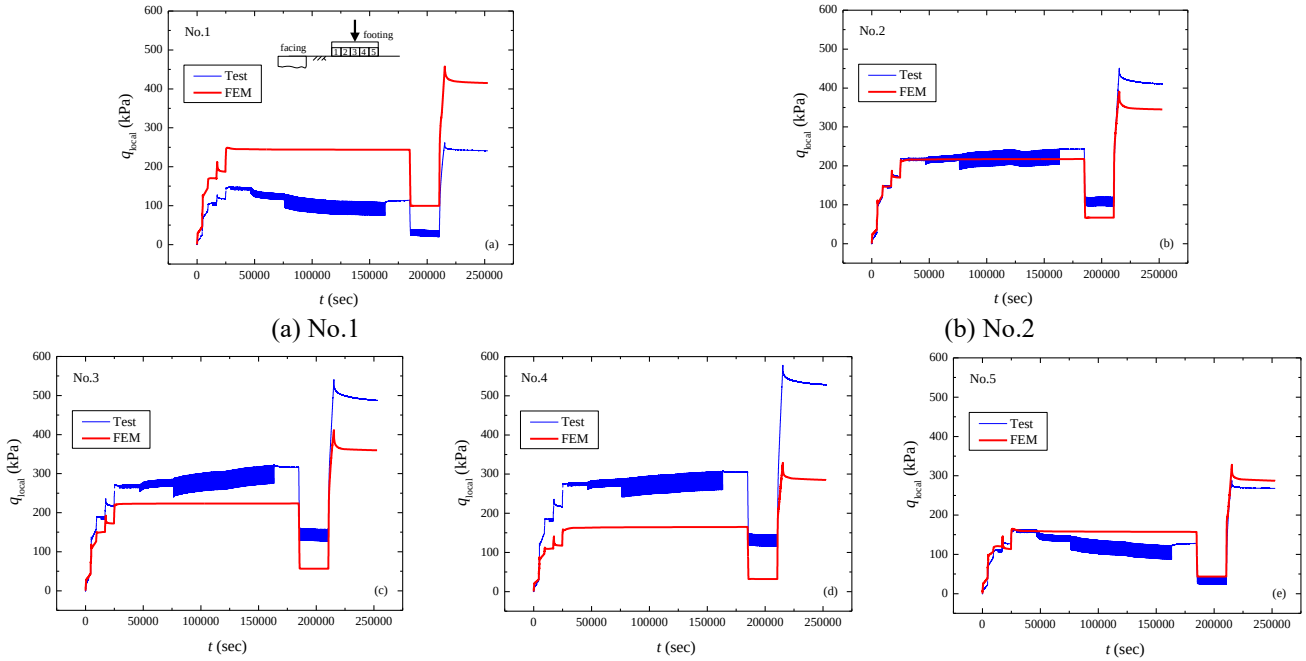

(a) No.1 (b) No.2

(c) No.3 (d) No.4 (e) No.5

Fig. 9 Comparisons of time histories of the local vertical stress of footing between FEM simulation and physical model test (RW-Test2)

the local tensile forces in geogrid arranged in retaining wall from both FEM simulation and physical model test are a parabola. The present FEM can capture the feature of the local tensile force along the distance, *d*, from the back of the facing. The values of tensile force from FEM simulation are also in good agreement with the measured ones in the physical model test in a period immediately after loading starts, but the predicted values become larger than the measured ones after state x. The location of the maximum of local tensile force can be predicted well by the presented FEM. The maximum value is always located beneath the right hand of the footing base.

Of particular note is that the predicted values in test RW-Test3 (Fig. 8) increase but the measured ones decrease after the state x. It can be seen from Fig. 6 that the average vertical footing pressure reaches the peak at the state L. Therefore, the simulated trend of tensile force is similar to the average vertical footing pressure, but the measured trend of tensile force is the opposite. In theory, the value of tensile force in reinforcement increases as the footing pressure increases. This peculiar experimental result may attribute to rupture of the other geogrid strand(s) of the same layer after the state x. Another related factor could be that shear bands have started developing from the footing edges, which may have increased the tensile forces in the upper reinforcement layers crossing the shear bands while may have decreases the tensile forces in the lower reinforcement layers that are located below the shear bands (including 5th layer of geogrid). This phenomenon may not be well captured in the present simulation.

4.4 Local stresses below the footing

The local stresses below the footing in the physical model test RW-Test2 were simulated. Figs. 9 and 10 show the time histories of the local vertical stress of footing, q_{local}, and the local shear stress of footing, $\tau_{vh,local}$, respectively. The positive direction of the local shear stress is defined as counter-clockwise. The experimental results are also presented. In Figs. 9-10, No.1, No.2, No.3, No.4 and No.5

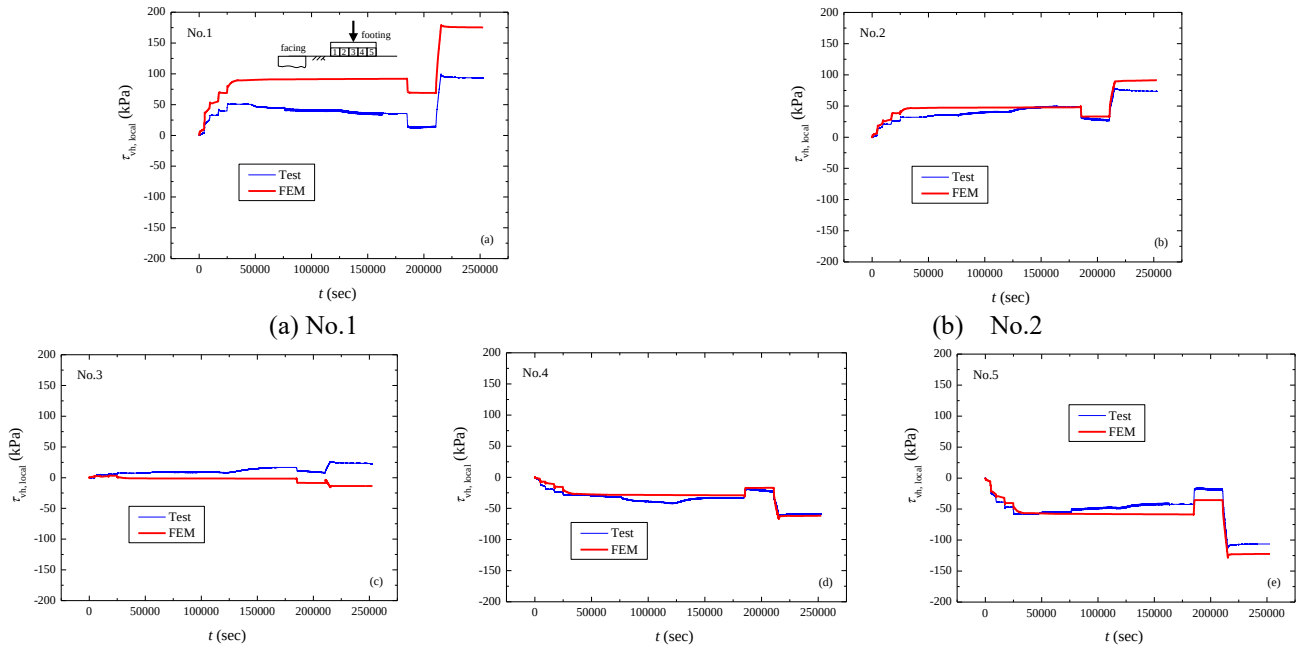

(a) No.1 (b) No.2

(c) No.3 (d) No.4 (e) No.5

Fig. 10 Comparisons of time histories of the local shear stress of footing between FEM simulation and physical model test (RW-Test2)

correspond to the position in sand immediately beneath the footing base from the left to the right.

It can be seen in Figs. 9 and 10 that the trends of jump in q_{local} and $\tau_{vh,local}$ upon the stepwise in the loading rate are well simulated. Despite a satisfactory simulation of the global *q-s-t* behavior, the local vertical stress of footing at the footing edge (No.1), close to the facing, is highly over-predicted while the values at No.3 (the footing center) and No.4 are under-predicted. For the local shear stress of footing, the value at the footing edge close to the facing is highly over-predicted while the value at the footing center is under-predicted. These inconsistencies may be caused by the different procedures of the applied load in the physical model test and the FEM simulation. That is, in the physical model tests, the load was applied through a 10 cm-wide rigid strip footing on the top surface of the back wall which was under a concentrated force by the piston rod. For this reason, the footing may have rotated slightly reducing the local load in load cell No. 1. In the FEM analysis, the loading was idealized in that the uniform vertical displacement was applied on the six nodes at the bottom of footing.

5. Conclusions

The time-dependent behaviors considering loading-rate effect of geosynthetic reinforced soil retaining walls were difficultly implemented in the past FEM analyses. The present FEM, embedding the elasto-viscoplastic properties of both backfill and geosynthetic reinforcements, achieves the success in the boundary value problems of geosynthetic reinforced soil retaining walls. Further studies should be performed to apply the FEM analysis technique to the practical engineering problems. By comparing the FEM simulation results with those from the physical model test results, the following conclusions can be drawn:

• It is shown that the results from the FEM simulations of geogrid reinforced sand retaining wall were in good agreement with the physical model test results with respect to the overall *q-s-t* relationships. In particular, the time effects on the *q-s* behavior observed in the physical model tests were well simulated. Moreover, the behavior of the high stiffness upon the stepwise changes in the loading rate, after the creep loading stages and stress relaxation stages could also be captured well by the presented nonlinear elasto-viscoplastic FEM analysis.

• The feature of the lateral earth pressure distributions from the back of retaining wall under the aforementioned various loading conditions can also be well simulated by the presented FEM. The distribution pattern of earth pressure was a triangle.

• The distribution feature of the local tensile force in geogrid reinforcement arranged in retaining wall can also be well simulated through the presented FEM. The distribution pattern of the local tensile force is a parabola. The maximum value is always located at the below of right hand of the footing base.

• The trends of jump in local stresses below the footing upon the step-changes in the loading rate are well simulated by the FEM, such as the local vertical stress and the local shear stress. However, the local stresses of the footing at the footing edge are highly over-predicted while the values at the footing center are under-predicted, despite a satisfactory simulation of the global *q-s-t* behavior.

Acknowledgments

The authors would like to express their sincere thanks to

Prof. Fangle Peng, a professor at Tongji University, for his discussions, and Dr. Daiki Hirakawa for sharing the data of model tests performed at Geotechnical Laboratory of the University of Tokyo. The authors acknowledge gratefully the support provided by the National Natural Science Foundation of China (51308533), the National Key Basic Research Program of China (2015CB251602), and the Fundamental Research Funds for the Central Universities (2019ZDPY18).

References

Bathurst, R.J., Nernheim, A., Walters, D.L., Allen, T.M., Burgess, P. and Saunders, D.D. (2009), "Influence of reinforcement stiffness and compaction on the performance of four geosynthetic-reinforced soil walls", *Geosynth. Int.*, **16**(1), 43-59. https://doi.org/10.1680/gein.2009.16.1.43.

Chen, C., McDowell, G. and Rui, R. (2018), "Discrete element modelling of geogrids with square and triangular apertures", *Geomech. Eng.*, **16**(5), 495-501. https://doi.org/10.12989/gae.2018.16.5.495.

Di Benedetto, H., Tatsuoka, F. and Ishihara, M. (2002), "Time-dependent shear deformation characteristics of sand and their constitutive modeling", *Soils Found.*, **42**(2), 1-22. https://doi.org/10.3208/sandf.42.2_1.

Elshesheny, A., Mohamed, M., Nagy, N.M. and Sheehan, T. (2020), "Numerical behaviour of buried flexible pipes in geogrid-reinforced soil under cyclic loading", *Comput. Geotech.*, **122**, 103493. https://doi.org/10.1016/j.compgeo.2020.103493.

Ezzein, F.M., Bathurst, R.J. and Kongkitkul, W. (2015), "Nonlinear load-strain modeling of polypropylene geogrids during constant rate-of-strain loading", *Polym. Eng. Sci.*, **55**(7), 1617-1627. https://doi.org/10.1002/pen.23999.

Han, J., Jiang, Y. and Xu, C. (2018), "Recent advances in geosynthetic-reinforced retaining walls for highway applications", *Front. Struct. Civ. Eng.*, **12**(2), 239-247. https://doi.org/10.1007/s11709-017-0424-8.

Helwany, M.B. and Wu, J.T.H. (1995), "A numerical model for analyzing long-term performance of geosynthetic-reinforced soil structures", *Geosynth. Int.*, **2**(2), 429-453. https://doi.org/10.1680/gein.2.0017.

Hirakawa, D. (2003), "Study on residual deformation characteristics of geosynthetic- reinforced soil structures", Ph.D. Dissertation, University of Tokyo, Tokyo, Japan.

Hirakawa, D., Kongkitkul, W., Tatsuoka, F. and Uchimura, T. (2003), "Time-dependent stress-strain behaviour due to viscous properties of geogrid reinforcement", *Geosynth. Int.*, **10**(6), 176-199. https://doi.org/10.1680/gein.10.6.176.37246.

Hoque, E. and Tatsuoka, F. (1998), "Anisotropy in elastic deformation of granular materials", *Soils Found.*, **38**(1), 163-179. https://doi.org/10.3208/sandf.38.163.

Hosseinpour, I., Riccio, M. and Almeida, M.S.S. (2014), "Numerical evaluation of a granular column reinforced by geosynthetics using encasement and laminated disks", *Geotext. Geomembranes*, **42**(4), 363-373. https://doi.org/10.1016/j.geotexmem.2014.06.002.

Karim, M.R., Manivannan, G., Gnanendran, C.T. and Lo, S.C.R. (2011), "Predicting the long-term performance of a geogrid-reinforced embankment on soft soil using two-dimensional finite element analysis", *Can. Geotech. J.*, **48**(5), 741-753. https://doi.org/10.1139/t10-104.

Karpurpu, R. and Bathurst, R.J. (1995), "Behaviour of geosynthetic reinforced soil retaining walls using the finite element method", *Comput. Geotech.*, **17**(3), 279-299. https://doi.org/10.1016/0266-352X(95)99214-C.

Kongkitkul, W., Chantachot, T. and Tatsuoka, F. (2014), "Simulation of geosynthetic load-strain-time behaviour by the non-linear three-component model", *Geosynth. Int.*, **21**(4), 244-255. https://doi.org/10.1680/gein.14.00012.

Kotake, N., Tatsuoka, F., Tanaka, T., Siddiquee, M.S.A. and Huang, C.C. (2002), "FEM simulation of the bearing capacity of level reinforced sand ground subjected to footing load", *Geosynth. Int.*, **8**(6), 501-549. https://doi.org/10.1680/gein.8.0205.

Kuwano, R. and Jardine, R.J. (2002), "On measuring creep behaviour in granular materials through triaxial testing", *Can. Geotech. J.*, **39**(5), 1061-1074. https://doi.org/10.1139/t02-059.

Lade, P.V., Liggio, J.C.D. and Nam, J. (2009), "Strain rate, creep, and stress drop-creep experiments on crushed coral sand", *J. Geotech. Geoenviron. Eng.*, **135**(7), 941-953. https://doi.org/10.1061/(ASCE)GT.1943-5606.0000067.

Li, F.L., Peng, F.L., Tan, Y., Kongkitkul, W. and Siddiquee, M.S.A. (2012), "FE simulation of viscous behavior of geogrid-reinforced sand under laboratory-scale plane-strain-compression testing", *Geotext. Geomembranes*, **31**, 72-80. https://doi.org/10.1016/j.geotexmem.2011.09.005.

Liu, H.B. and Won, M.S. (2009), "Long-term reinforcement load of geosynthetic-reinforced soil retaining walls", *J. Geotech. Geoenviron. Eng.*, **135**(7), 875-889. https://doi.org/10.1061/(ASCE)GT.1943-5606.0000052.

Liu, H.B., Wang, X.Y. and Song, E.X. (2009), "Long-term behavior of GRS retaining walls with marginal backfill soils", *Geotext. Geomembranes*, **27**(4), 295-307. https://doi.org/10.1016/j.geotexmem.2009.01.002.

Ortiz, M. and Simo, J.C. (1986), "An analysis of a new class of integration algorithms for elastoplastic constitutive relations", *Int. J. Numer. Meth. Eng.*, **23**(3), 353-366. https://doi.org/10.1002/nme.1620230303.

Peng, F.L., Kotake, N., Tatsuoka, F., Hirakawa, D. and Tanaka, T. (2000), "Plane strain compression behaviour of geogrid-reinforced sand and its numerical analysis", *Soils Found.*, **40**(3), 55-74. https://doi.org/10.3208/sandf.40.3_55.

Peng, F.L., Li, F.L., Tan, Y. and Kongkitkul, W. (2010), "FEM simulation of viscous properties for granular materials considering the loading rate effect", *Granul. Matter*, **12**(6), 555-568. https://doi.org/10.1007/s10035-010-0194-7.

Peng, F.L., Siddiquee, M.S.A., Tatsuoka, F., Yasin, S.J.M. and Tanaka, T. (2009), "Strain energy-based elasto-viscoplastic constitutive modelling of sand for numerical simulation", *Soils Found.*, **49**(4), 611-629. https://doi.org/10.3208/sandf.49.611.

Pham Van Bang, D., Di Benedetto, H., Duttine, A. and Ezaoui, A. (2007), "Viscous behaviour of dry sand", *Int. J. Numer. Anal. Met.*, **31**(15), 1631-1658. https://doi.org/10.1002/nag.606.

Rowe, R.K. and Skinner, G.D. (2001), "Numerical analysis of geosynthetic reinforced retaining wall constructed on a layered soil foundation", *Geotext. Geomembranes*, **19**(7), 387-412. https://doi.org/10.1016/s0266-1144(01)00014-0.

Rowe, R.K. and Taechakumthorn, C. (2011), "Design of reinforced embankments on soft clay deposits considering the viscosity of both foundation and reinforcement", *Geotext. Geomembranes*, **29**(5), 448-461. https://doi.org/10.1016/j.geotexmem.2011.03.001.

Safa, M., Maleka, A., Arjomand, M.A., Khorami, M. and Shariati, M. (2019), "Strain rate effects on soil-geosynthetic interaction in fine-grained soil", *Geomech. Eng.*, **19**(6), 523-532. https://doi.org/10.12989/gae.2019.19.6.523.

Shi, W.Z., Peng, F.L. and Kongkitkul, W. (2016), "FE simulation of rate-dependent behaviours of polymer geosynthetic reinforcements for an estimation of mobilized tensile force in a reinforced soil", *Comput. Geotech.*, **80**, 49-58. https://doi.org/10.1016/j.compgeo.2016.06.005.

Siddiquee, M.S.A., Noguchi, T. and Hirakawa, D. (2015), "Computational simulation of time-dependent behavior of soil-structure interaction by using a novel creep model: Application to a geosynthetic-reinforced soil physical model", *Comput. Geotech*., **66**, 180-188. https://doi.org/10.1016/j.compgeo.2015.02.001.

Siddiquee, M.S.A., Tanaka, T. and Tatsuoka, F. (1995), "Tracing the equilibrium path by dynamic relaxation in materially nonlinear problems", *Int. J. Numer. Anal. Met.*, **19**(11), 749-767. https://doi.org/10.1002/nag.1610191102.

Siddiquee, M.S.A., Tanaka, T. and Tatsuoka, F. (2006), "FEM simulation of the viscous effects on the stress-strain behaviour of sand in plane strain compression", *Soils Found*., **46**(1), 99-108. https://doi.org/10.3208/sandf.46.99.

Tanaka, T. and Kawamoto, O. (1988), "Three dimensional finite element collapse analysis for foundations and slopes using dynamic relaxation", *Proceedings of the 6th International Conference on Numerical Methods in Geomechanics*, Innsbruck, Austria, April.

Tatsuoka, F., Hirakawa, D., Shinoda, M., Kongkitkul, W. and Uchimura, T. (2004), "An old but new issue; viscous properties of polymer geosynthetic reinforcement and geosynthetic-reinforced soil structures", *Proceedings of the 3rd Asian Regional Conference on Geosynthetics*, Seoul, Korea.

Tatsuoka, F., Ishihara, M., Di Benedetto, H. and Kuwano, R. (2002), "Time-dependent shear deformation characteristics of geomaterials and their simulation", *Soils Found*., **42**(2), 103-129. https://doi.org/10.3208/sandf.42.2_103.

Villard, P., Kotake, N. and Otani, J. (2002), "Modelling of reinforced soil in finite element analysis", *Proceedings of the 7th International Conference on Geosynthetics*, Nice, France, September.

CC